Article

NaYF4:Yb,Er Upconversion Nanotransducer with In-Situ Fabrication of Ag2S for Near-Infrared Light Responsive Photoelectrochemical Biosensor

Zhenli Qiu, Jian Shu, and Dianping Tang

Anal. Chem., **Just Accepted Manuscript** • DOI: 10.1021/acs.analchem.8b03446 • Publication Date (Web): 17 Sep 2018

$NaYF_4$:Yb,Er Upconversion Nanotransducer with In-Situ Fabrication of Ag_2S for Near-Infrared Light Responsive Photoelectrochemical Biosensor

Zhenli Qiu, Jian Shu, and Dianping Tang*

Key Laboratory of Analytical Science for Food Safety and Biology (MOE & Fujian Province), State Key Laboratory of Photocatalysis on Energy and Environment, Department of Chemistry, Fuzhou University, Fuzhou 350116, People's Republic of China

*Corresponding Author: Phone: +86-591-2286 6125. Fax: +86-591-2286 6135. E-mail: dianping.tang@fzu.edu.cn.

ABSTRACT: An innovative near-infrared (NIR) light-driven photoelectrochemical (PEC) aptasensor was constructed for sensitive screening of carcinoembryonic antigen (CEA) on the basis of *in-situ* formation of Ag_2S nanoparticles on the $NaYF_4$:Yb,Er upconversion nanoparticles (UCN), coupling with hybridization chain reaction (HCR) for the signal amplification. Utilization of UCN as the light nanotransducer could convert the NIR light into an applicable wavelength harvested by semiconductors. The multiemissions of $NaYF_4$:Yb,Er UCN could match well with the absorption characteristics of Ag_2S. In the presence of target CEA, a sandwich-type reaction was carried out between capture CEA aptamer/$NaYF_4$:Yb,Er-modified electrode and trigger CEA aptamer, which underwent an unbiased strand-displacement reaction to open C-rich hairpin probes in sequence between two alternating hairpins with the assistance of C-Ag^+-C chelation reaction. Upon addition of sulfidion, the chelated Ag^+ ions in the long-nicked DNA poly strands by hybridization chain reaction reacted with S^{2-} to generate Ag_2S nanoparticles. The formed Ag_2S could utilize effectively the upconversion emissions to amplify the photocurrent. Under optimal conditions, $NaYF_4$:Yb,Er-based NIR light-responsive PEC aptasensing platform exhibited high sensitivity for the determination of CEA within a dynamic linear range of 0.005 – 5.0 ng mL^{-1}. The limit of detection was 1.9 pg mL^{-1}. Good precision and high specificity could be acquired in this system for the analysis of target CEA. Human serum samples containing target CEA were measured by using our strategy, and received well-matched results relative to human CEA enzyme-linked immunosorbent assay kits. Importantly, $NaYF_4$:Yb,Er-based NIR light-responsive PEC aptasensing system provides a new ideal on the detection of disease-related biomarkers by using nucleic acid-based amplification strategy.

Photoelectrochemical (PEC) biosensor, a high-efficient sensing technique by coupling with electrochemistry and photochemistry, has attracted increasing attention for the detection of various biomolecules in the direction of standardization, modularization and generalization in recent years.[1-3] Typically, PEC biosensors usually rely on introduction of the photoinduced electron/hole in photoactive materials by light excitation to transfer it to the electrode interface, thus causing the change of the output photocurrent signal.[2,3] Selection of photoactive materials is a crucial factor associated with the analytical performance of PEC biosensors.[4,5] Nowadays, different photoactive materials, mainly metal semiconductors (*e.g.*, TiO_2, ZnO, and CdS) have been employed for the fabrication of PEC biosensors.[6-8] However, one disadvantage of using metal semiconductors depends on the narrow photoabsorption regions, which can only employ ultraviolet (UV) light as the light sources, thereby limiting their wide application.[9-11] Therefore, exploring some innovative photoactive materials would be advantageous for the development of advanced photoelectrochemical biosensing platforms.

Upconversion (UC) refers to the multiphoton energy transfer process in which the low-energy photons (mainly near-infrared, NIR, light) can be converted into the high-energy photons (UV light or visible light).[12,13] Under the low-energy NIR light illumination, the auto-fluorescence background of samples can be efficiently eliminated. Moreover, high resistance to photo-induced bleaching seems to minimize the light scattering, whilst NIR light can protect biological substance from photo-damage.[14,15] In contrast, upconversion nanoparticle (UCN) has been often used as an efficient nanotransducer for the applications in bioimagings, photocatalysts, fluorescence biosensors, and photodynamic therapy.[16-19] Li *et al*. employed the natural bio-microlens to greatly enhance fluorescence intensity of core-shell UCN@SiO_2-NH_2 nanoparticles.[20] Xu *et al*. combined the plasmonic gold, upconversion nanoparticles with porous titanium dioxide to synthesize core-shell UCN@TiO_2-Au microspheres for the creation of

high-activity hybrid photocatalyst.[21] Recently, our group developed a NIR-to-UV light-mediated photoelectrochemical aptasensor based

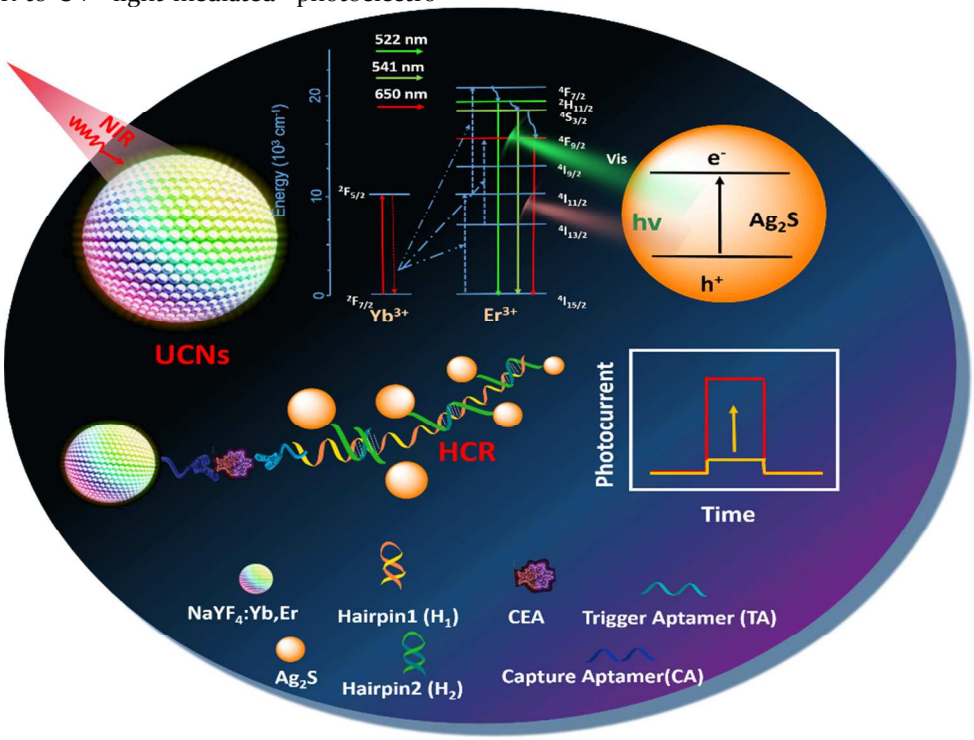

Scheme 1. Schematic illustration of $NaYF_4$:Yb,Er upconversion nanoparticle (UCN)-based near-infrared (NIR) light-responsive photoelectrochemical (PEC) aptasensor to detect carcinoembryonic antigen (CEA) by coupling with target-triggered hybridization chain reaction (HCR) between hairpin DNA1 (H_1) and hairpin DNA2 (H_2), accompanying *in-situ* formation of Ag_2S nanoparticles on the basis of typical C-Ag^+-C chelation reaction for the signal amplification.

on core-shell $NaYF_4$:Yb,Tm@TiO_2 UCNs, accompanying DNA-based amplification strategy.[22] Unfavorably, our recent research found that TiO_2 shells could only harvest the UV and blue emissions from $NaYF_4$:Yb,Tm UCNs. Actually, Yb^{3+}-doped $NaYF_4$ as a sensitizer primarily adsorbed at 980 nm. Subsequently the activator Tm^{3+} ions gave the multiemissions (UV and visible emissions). In this regard, $NaYF_4$:Yb,Tm@TiO_2 system lacked the capacity to adequately take advantage of all the multi-emissions from upconversion process. Inspiringly, Ag_2S, a narrow band gap (about 1.1 eV) and the absorption capacity of the whole visible (Vis) region, is a promising candidate as the photoactive material for design of UCN-based PEC system due to its high flexibility to choice the excitation wavelength.[23,24] In addition, Ag_2S has negligible toxicity without the existence of any toxic ions (*e.g.*, Hg^{2+}, Pb^{2+}, and Cd^{2+}). Importantly, the solubility product constant of Ag_2S exhibits an ultra-low value (Ksp = 6.3×10^{-50}), which facilitates *in-situ* generation of brown Ag_2S precipitation in the minimum concentration of Ag^+.[25] To this end, our motivation of this study is to combine upconversion nanoparticles with Ag_2S semiconductor for the development of NIR light responsive photoelectrochemical sensing system.

Carcinoembryonic antigen (CEA) is a kind of specific cancer biomarker, associated with the early diagnosis of colon and rectal cancer.[26] Massive clinical data showed that the value of CEA increased in bowel cancer, but also in the serum of breast cancer, lung cancer and other malignant tumors.[27] Although it cannot be used as a specific indicator of malignancy diagnosis, it still has important clinical value in the differential diagnosis, monitoring and curative effect evaluation of malignant tumor.[28] In this contribution, we design an advanced PEC sensing protocol to determinate CEA on the $NaYF_4$:Yb,Er UCNs (Scheme 1). The signal is amplified by coupling with hybridization chain reaction and formation of Ag_2S nanoparticles under near-infrared light irradiation. The directional light emission can be produced by adjustment of lanthanide dopant. Er^{3+} and Yb^{3+}-codoped $NaYF_4$ (UCN; as the energy donor) can convert NIR light into Vis light associated with the matched absorption of Ag_2S. First, the NIR light-driven PEC aptasensor is fabricated through dropping poly(ethylenimine) (PEI)-functionalized UCNs on the fluorine-tin oxide electrode, followed by conjugation with capture CEA aptamer (CA) using maleimide derivatization as the cross-linkage agent. To detect target CEA, a sandwiched reaction mode is initially carried out between the immobilized capture aptamer on the electrode and trigger CEA aptamer (TA). In this regard, the carried trigger stand promotes the hybridization chain reaction between cytosine-rich (C-rich) hairpin probes to expose the repeated units of cytosine-rich (C-rich) DNA stands for the C-Ag^+-C chelation in the presence of silver ions. Then, the deposition of Ag_2S is generated *in-situ* by means of the interaction between Ag^+ and S^{2-} ions, which can absorb Vis region from $NaYF_4$:Yb,Er for the amplified

photocurrent. NIR light-driven PEC aptasensor for the CEA detection based on the *in-situ* reaction of Ag_2S endows a new concept of development for PEC sensing strategy to improve the efficiency of UCN emission.

EXPERIMENTAL SECTION

Preparation of PEI-Functionalized $NaYF_4$:Yb,Er Upconversion Nanoparticles. The PEI-functionalized $NaYF_4$:Yb,Er UCNs (denoted as PEI-UCNs) were prepared according to the previous report with some modification.[29] Initially, 1.0 mmol of lanthanide chloride mixture including $YCl_3 \cdot 6H_2O$, $YbCl_3 \cdot 6H_2O$, $ErCl_3 \cdot 6H_2O$ (molar ratio, Y : Yb : Er = 78 : 20 : 2) and NaCl (2.0 mmol) were dissolved in 15 mL of ethylene glycol (EG) solution. Thereafter, another EG solution (10 mL) including NH_4F (4.0 mmol) and PEI (0.25 g) was added dropwise into the above-resulting mixture, and vigorously stirred for another 20 min. Following that, the mixture was thrown into a Teflon-lined autoclave. The product was heated for 2 h at 200 °C. At last, the white precipitate was collected by centrifugation (10 min, 13,000*g*), washed with ethanol and ultrapure water alternately, and dried at 60 °C for use.

Fabrication of NIR Light-Driven PEC Aptasensor. Prior to fabrication, a fluorine-tin oxide (FTO) glassy electrode with an active area of 28.26 mm^2, prepared by using a waterproof tape with a circle hole (3.0 mm in radius), was initially pretreated by using NaOH (1.0 M) and 10% H_2O_2, respectively. Then, 20 μL of PEI-UCN aqueous suspension (2.0 mg mL^{-1}) was dropped onto the hole, and naturally dried at 25 °C. After that, 50 μL of sulfosuccinimidyl 4-(*N*-maleimidomethyl) cyclohexane-1-carboxylate (Sulfo-SMCC; 0.5 mg mL^{-1}, dispersed in HEPES buff, pH 7.4, 10 mM) was cast on PEI-UCN-modified electrode, and incubated for 60 min at 25 °C. The resultant electrode was washed with HEPES buffer to remove the excess Sulfo-SMCC. Subsequently, the resulting FTO electrode was activated with maleimide, and reacted overnight with the thiolated capture CEA aptamer (CA) (20 μL, 3.0 μM) at 25 °C. The modified electrode was washed as before. Finally, the photosensitive electrode was incubated for 60 min at RT with 2.5 wt % BSA aqueous solution to eliminate the possible active site on the upconversion nanoparticles, and stored at 4 °C when not in use.

Reaction Protocol with Target CEA. The aptasensor was used to detect target analyte as follow. Prior to reaction with the aptasensor, a 50-μL incubation solution was prepared by mixing different-concentration target CEA, 3.0 μM trigger aptamer (TA), 3.0 mM $AgNO_3$, 1.0 μM hairpin DNA1 (H_1) with 1.0 μM hairpin DNA2 (H_2). Following that, the mixture was quacking dropped on the aptasensor, and reacted for 2.5 h at 37 °C. During this process, a sandwiched reaction was implemented between the trigger aptamer and capture aptamer. Also, another two reactions including target-triggered hybridization chain reaction between hairpins DNA1 and DNA2. Simultaneously the C-Ag^+-C chelation reaction were carried out. Subsequently, the resultant electrode was washed with HEPES buff (10 mM, pH 7.4). Finally, the as-prepared electrode was used for photoelectrochemical measurement after reaction with Na_2S (Please see the detailed PEC detection process in the Supporting Information)

RESULTS AND DISCUSSION

Characterization of $NaYF_4$:Yb,Er Upconversion Nanoparticles. Taking the advantages of upconversion characteristics of lanthanide ions (Ln^{3+})-doped nanoparticles, an advanced aptasensing platform is designed, coupling *in-situ* generation of Ag_2S nanoparticles with target-triggered hybridization chain reaction, followed by the near-infrared light-driven photoelectrochemical measurement (Scheme 1). As expected, introduction of $NaYF_4$:Yb,Er-based upconversion nanoparticles is served as the versatile light nanotransducer, which can efficiently convert the near-infrared light into the suitable wavelengths. In addition, the *in-situ* formation of Ag_2S nanoparticles on target-triggered HCR products can absorb the emissions from upconversion nanoparticles, thereby resulting in the increasing photocurrent. With the increasing of target CEA concentration in the sample, the product by hybridization chain reaction increased, thus chelating numerous silver ions by the C-Ag^+-C reaction. Upon addition of sulfion (S^{2-}) ions, the formed Ag_2S nanoparticles increased to promote the increment of photocurrent under the near-infrared light irradiation. By calculating the photocurrent, we can exactly evaluate the CEA level in the sample.

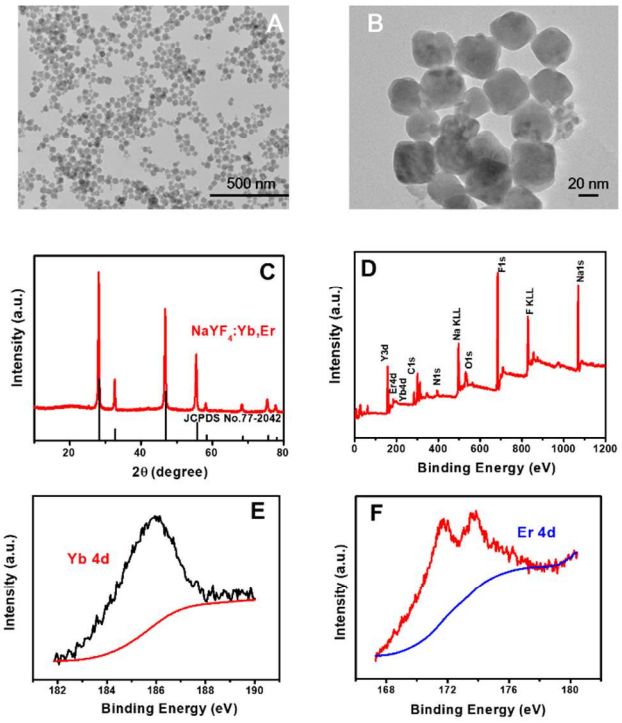

Figure 1. (A) TEM, (B) HRTEM, (C) XRD patterns and (D) full XPS spectra of PEI-functionalized $NaYF_4$:Yb,Er up-

conversion nanoparticles; and (E,F) the high-resolution XPS spectra of (E) Yb 4d and (F) Er 4d.

To realize our design, the successful synthesis of PEI-functionalized $NaYF_4$:Yb,Er nanostructures is very crucial for the development of NIR light-driven PEC aptasensing system. Typically, branched PEI has numerous free amine groups and high affinity for the conjugation with Ln^{3+} ion. Moreover, PEI-functionalized UCNs exhibit high water-solubility and numerous active sites for the labeling of biomolecules. First, we used high-resolution transmission electron microscopy (HRTEM; Tecnai G2 F20 S-TWIN FEI, USA) to characterize the morphology and structure of the as-synthesized upconversion nanoparticles. As indicated in Figure 1A and Figure 1B, PEI-UCNs were nearly spherical, and the average size was ~40 nm in diameter. Obviously, $NaYF_4$:Yb,Er upconversion nanoparticles could be homogenously dispersed in ultrapure water, suggesting good water-solubility. Next, the crystalline structure of upconversion nanoparticles was investigated by using powder X-ray diffraction (XRD; DY5261/Xpert3 CEM, USA). As seen from Figure 1C, the crystal structure of UCNs was indexed to the standard XRD pattern of cubic phase $NaYF_4$ (JCPDS no.77-2042), indicating that the doped lanthanide ions did not damage the inner structure.[30] The chemical composition and states of the existing elements were monitored by X-ray photoelectron spectroscopy (XPS; Scientific ESCALAB 250 spectrometer, USA). As indicated in Figure 1D, all the elements including Na, Y, F, Yb and Er were existed in the nanostructures. Furthermore, the high-resolution XPS spectra also gave the characteristic peak of Yb 4d at 185.96 eV (Figure 1E) and two characteristic peaks at 173.55 and 175.0 eV for Er 4d (Figure 1F), indicating the successful co-doping of Yb^{3+} and Er^{3+} ions into $NaYF_4$ crystals.[31] These results revealed that $NaYF_4$:Yb,Er-based upconversion nanoparticles could be successfully synthesized by our designed route.

Evaluation of Feasibility. For the development of Ag_2S-deposited $NaYF_4$:Yb,Er upconversion nanoparticles by C-Ag^+-C chelation and the *in-situ* chemical reaction, the surface topologies of the modified electrodes were characterized by using an inverted metallurgic microscopy (MSD400; CCD; HT1600CN, Optec, China) before and after reaction with target CEA, trigger aptamer, H_1, H_2, Ag^+ and S^{2-}. Figure 2a gives typical microscope image of $NaYF_4$:Yb,Er UCNs-modified FTO electrode at bright field. For comparison, the microscope image of Ag_2S nanoparticles alone, deposited on the cleaned FTO electrode, was monitored, which exhibited rough brown-yellow structure (Figure 2B). After reaction with the C-Ag^+-C chelation, however, a rough surface was observed in Figure 2C, indicating that the chelated silver ions between cytosine bases could react with the added S^{2-} ions to generate the Ag_2S nanoparticles and coated on the surface of $NaYF_4$:Yb,Er UCNs. The results were almost in accordance with those obtained from scanning electron microscopy (SEM) (please see Figure S1 and the corresponding description in the Supporting Information). Curve '*a*' in Figure 2D shows UV-vis absorption spectroscopy of hairpin DNA1 and hairpin DNA2 after reaction with Ag^+ and S^{2-} ions, and no characteristic absorption peaks were observed from 400 nm to 1000 nm. As seen from curves '*b*-*c*', the formed Ag_2S nanoparticles could absorb the emissions of $NaYF_4$:Yb,Er UCNs to transform NIR light into Vis light. Moreover, the generated Ag_2S had a broad absorption range in the visible region (curve '*a*') due to its low band gap (approximately 1.1 eV), which overlapped with the emission peaks (curve '*b*') of Vis light (531 nm, 546 nm and 662 nm) from UCNs corresponding to the $^2H_{11/2} \rightarrow {}^4I_{15/2}$, $^4S_{3/2} \rightarrow {}^4I_{15/2}$ and $^4F_{9/2} \rightarrow {}^4I_{15/2}$ transition of Er^{3+}.[32,33] In contrast, the intensity of the emission peaks exhibited a sharp deceleration and even disappear after the formation of Ag_2S nanoparticles (curve '*c*'). These results suggested that Ag_2S nanoparticles could absorb the Vis light from $NaYF_4$:Yb,Er UCNs to provide the photo-generated electrons-holes pair.

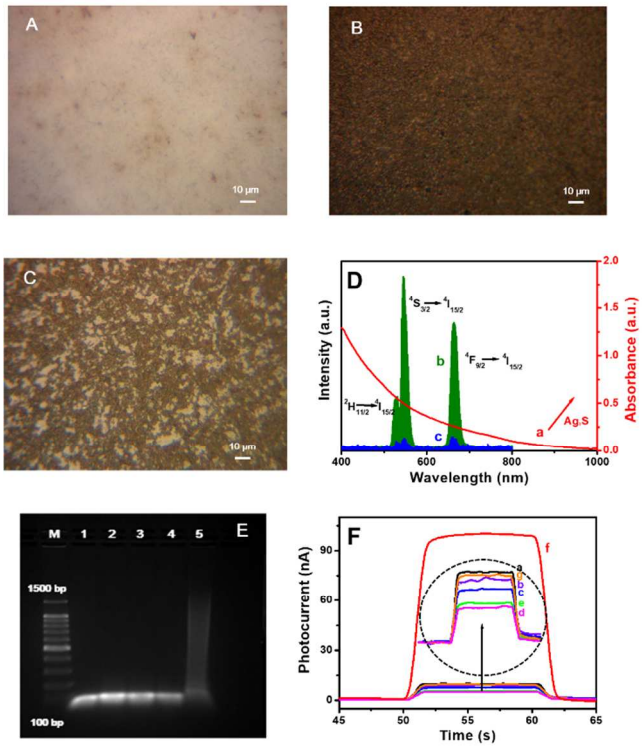

Figure 2. (A,B,C) The inverted metallurgic microscope images of (A) PEI-$NaYF_4$:Yb,Er UCNs, (B) Ag_2S precipitate alone and (C) *in-situ* growth of Ag_2S on PEI-$NaYF_4$:Yb,Er UCNs; (D) UV-Vis absorption spectra of Ag_2S (*a*), and (*b*,*c*) upconversion photoluminescence spectra of (*b*) $NaYF_4$:Yb,Er and (*c*) *in-situ* growth of Ag_2S on $NaYF_4$:Yb,Er UCNs; (E) Agarose gel electrophoresis (1.0%) image (M: marker, lane 1: 1.0 μM H_1, lane 2: 1.0 μM H_2, lane 3: 1.0 μM H_1 + 1.0 μM H_2, lane 4: 1.0 μM H_1 + 1.0 μM H_2+ 0.1 μM CA, lane 5: 1.0 μM H_1 + 1.0 μM H_2+ 0.1 μM TA); (F) Photocurrents of (*a*) $NaYF_4$:Yb,Er UCNs, (*b*) UCNs + CA, (*c*) UCNs + CA + 0.01 ng mL^{-1} CEA + TA, (*d*) UCNs + CA + 0.01 ng mL^{-1} CEA + TA + H_1 + H_2, (*e*) sensor '*d*' + Ag^+, (*f*) sensor '*e*' + S^{2-} and (*g*) UCNs + CA + 0 ng mL^{-1} CEA + TA + H_1 + H_2 on the FTO electrode under NIR light excitation.

As mentioned above, the amplification of the detectable signal for NIR light-driven PEC aptasensing system derived from target-triggered hybridization chain reaction, accompanying the C-Ag^+-C chelation in the long-nicked DNA poly strands for the *in-situ* generation of Ag_2S nanoparticles. In this regard, the formation of long-nicked DNA strands were very important for the subsequent development during numerous Ag_2S formation. To demonstrate this issue, we employed agarose gel electrophoresis to monitor different products during the reaction (Figure 2E). Lane 1 and lane 2 represent the gel electrophoresis images of hairpins DNA1 and DNA2, respectively. In the absence of trigger aptamer, however, mixture of hairpins DNA1 and DNA2 did not cause their hybridization reaction because only one spot similar to that of hairpins DNA1 or DNA2 was observed at lane 3. In contrast, introduction of capture CEA aptamer in this system including hairpins DNA1 and DNA2 did not cause the reaction of strand hybridization, as shown in lane 4. When hairpins DNA1 and DNA2 were incubated with trigger aptamer, significantly, an obvious hybridization chain reaction was acquired (lane 5). These results indicated that hybridization chain reaction could be triggered by trigger CEA aptamer between hairpins DNA1 and DNA2. Because of specific CEA-aptamer reaction, target-triggered HCR could cause the formation of long-nicked DNA poly strands.

Logically, a question arises as to whether this system could be used to photoelectrochemically detect the analyte by NIR light-driven aptasensing strategy. Therefore, we investigated the photocurrent variations of this system at different stages (Figure 2F) for detection of 0.01 ng mL^{-1} CEA. As seen from curve '*a*', a relative weak photocurrent was obtained at $NaYF_4$:Yb,Er UCNs-modified FTO electrode, indicating that upconversion nanoparticles alone had a background signal, which could provide a convenience for fabrication of signal-on sensing platform. Moreover, the photocurrents gradually decreased after the modified electrode was conjugated with capture aptamer (curve '*b*'), and 0.01 ng mL^{-1} CEA + trigger aptamer (curve '*c*') in sequence, suggesting that the biomolecules with weak conductivity hindered the electron transfer. Similarly, introduction of hairpins DNA1 and DNA2 further decreased the photocurrent of the resulting electrode (curve '*d*'). In contrast, the photocurrent slightly increased after the chelation of silver ions with the C-rich bases (curve '*e*'). The reason might be most likely as a consequence of the fact that the formed C-Ag^+-C structure decrease the steric hindrance of long-nicked double-stranded DNA. When the resulting electrode reacted with S^{2-} ions, significantly, the photocurrent heavily increased (curve '*f*') in comparison with background signal. The increased photocurrent was ascribed to the fact that upconversion nanoparticles could transform NIR light into Vis light for the harvest of Ag_2S nanoparticles, thereby resulting in the increasing of the photocurrent. During this process, the added S^{2-} ion triggered the growth of Ag_2S by the chelated Ag^+ ion between cytosine bases on the basis of the common chemical reaction ($2Ag^+ + S^{2-} \rightarrow Ag_2S$). To further elucidate the harvest efficiency of Ag_2S nanoparticles during this process, Ag_2S nanoparticles alone were synthesized on the surface of the electrode by using our designed oligonucleotide strands, and the photocurrent was detected. As shown in Figure S2 in the Supporting Information, a relatively weak photocurrent was obtained in comparison with that of Ag_2S/$NaYF_4$:Yb,Er UCNs, indicating that Ag_2S nanoparticles or /$NaYF_4$:Yb,Er UCNs alone could not cause the strong photocurrent. Maybe, another puzzling question should be investigated whether the strong photocurrent stemmed from the non-specific absorption toward trigger CEA aptamer. As control test, this system was utilized to assay 0 ng mL^{-1} CEA with the same assay mode. As seen from curve '*g*', the photocurrent was similar with curve '*b*', suggesting that the change in the signal was attributed to the specific CEA-aptamer reaction. Hence, NIR light-driven $NaYF_4$:Yb,Er-modified aptasensing platform could be preliminarily utilized for the photoelectrochemical determination of target CEA

Optimization of Experimental Conditions. As described above, experimental conditions and external factors would affect analytical performance of NIR light-driven PEC aptasensor, *e.g.*, concentration of capture aptamer, incubation time CEA-triggered HCR with C-Ag^+-C structure and Na_2S concentration. First, we investigated the effect of CA concentration on the photocurrent of this system because target CEA capture on the electrode and progression of subsequent reactions heavily depended on the capture efficiency of the as-prepared aptasensor. A low-intensity CA was unfavorable for target CEA capture, whereas a high-intensity CA possibly decreased the capture ability because of the steric hindrance. As shown in Figure 3A, the maximum photocurrent was obtained at 3.0-μM capture aptamer by using 0.01 ng mL^{-1} CEA as an example. So, 3.0 μM of capture aptamer was used for the preparation of the aptasensor.

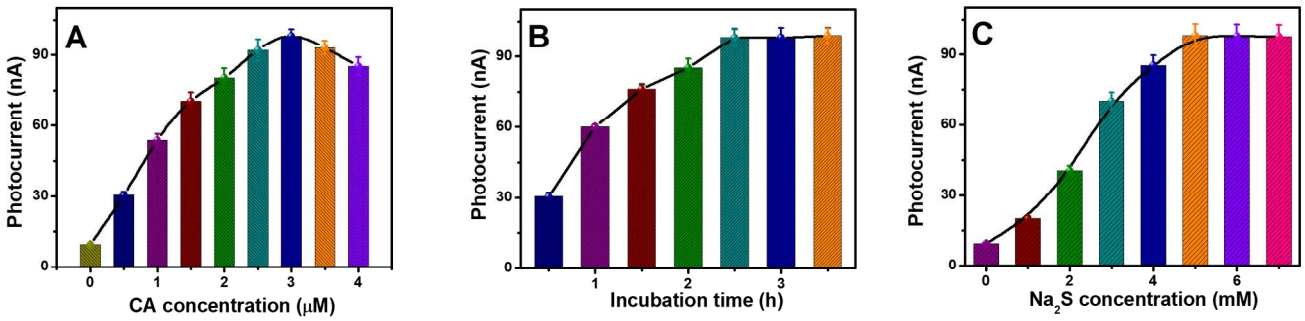

Figure 3. Influence of (A) CA concentration, (B) reaction time of CEA-triggered HCR with C-Ag^+-C structure, and (C) Na_2S concentration on the photocurrent of photoelectrochemical aptasensor under NIR light irradiation (0.01 ng mL^{-1} CEA and 2.0 mg mL^{-1} $NaYF_4$:Yb,Er UCNs used in these cases).

Next, we monitored the effect of incubation time during the reaction process with target CEA, trigger aptamer, H_1, H_2 and Ag^+ on the photocurrent of this system. Figure 3B gives the experimental results. As shown in Figure 3B, the current increased with incubation time aged, and reached the maximum signal after 2.5 h. Such a long incubation time might be due to the fact that it took some time to execute the hybridization chain reaction and CEA-aptamer reaction. To save the assay time, 2.5 h was selected as the incubation time with the incubation solution.

In addition, Na_2S concentration is also very important for the formation of Ag_2S nanoparticles, especially at high-concentration target CEA, since a large number of silver ions were chelated in the long-nicked DNA strands. Moreover, a low-amount Na_2S might take a longer time for the chelation reaction. As displayed in Figure 3C, the photocurrent reached a plateau after 5.0-mM Na_2S. Thus, 5.0 mM of Na_2S was utilized during the formation of Ag_2S nanoparticles.

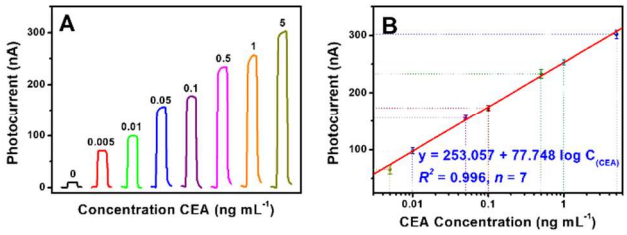

Figure 4. (A) Photocurrents of NIR light-driven PEC detection system toward CEA, using $NaYF_4$:Yb,Er UCNs as the matrices, accomanying target-triggered HCR and Ag_2S formation under NIR light irradiation; and (B) calibration plots.

Dose Responses of NIR Light-Driven Photoelectrochemic al Aptasensor toward Target CEA. By using the as-prepared $NaYF_4$:Yb,Er upconversion nanoparticles, the aptasensors were used to quantitatively determine CEA standards at various conentrations under the optimum conditions, using target-triggered hybridization chain reaction with the *in-situ* formation of Ag_2S nanoparticles, under NIR light irradiation. Figure 4A displays the signals of this systme toward target CEA, and the photocurrents increased with the increment of the analyte concentration. The linear curve could be obtained from 0.005 to 5 ng mL^{-1} (Figure 4B) as the following equantion: y (nA) = 253.057 + 77.748 × log$C_{[CEA]}$ (ng mL^{-1}) (R^2 = 0.996, n = 7). The limit of detection (LOD) was 1.9 pg mL^{-1} at $3\sigma/k$ (where σ is the standard deviation for eleven blank solution, and k is the slope of calibration plot). To further elucidate the advantages of this system by coupling upconversion nanoparticles with hybridization chain reaction, the linear range and LOD of our strategy were compared with other CEA detection schemes (Table S1 in the Supporting Information). A relatively good analytical performance could be acquired with our strategy. Such a low LOD should be ascribed to Ag_2S-based signal enhancement and HCR-based signal amplification. In addition, the threshold (cutoff) value of CEA is 3.0 ng mL^{-1} in human serum specimens.[34] Therefore, our strategy can meet the requirement of clinical diagnostics for target CEA.

Selectivity, Stability and Reproducibility. In this system, the specificity, reproducibility and stability are very important in the practical application. The selectivity of this method was implemented by assaying other biomarkers possible present in human serums, *e.g.*, alpha-fetoprotein (AFP), lysozyme (Lyso), human IgG, prostate-specific antigen (PSA), and thrombin (TB). The judgment was carried out by comparing with their photocurrents alone or coexistence. 0.01 ng mL^{-1} target CEA and 100-fold high-concentration nontarget (1.0 ng mL^{-1}) were utilized in these cases. All the photocurrents of this system toward nontarget analytes including AFP, Lyso, IgG, PSA and TB were close to the background signal (Figure 5). A strong signal was registered toward CEA. Importantly, the mixture containing CEA and other interfering biomarkers did not increase the signal. Therefore, the specificity of NIR light-driven PEC aptasensing system is satisfactory.

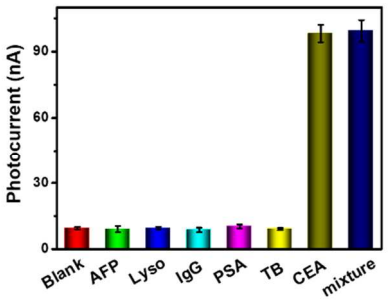

Figure 5. The specificity of NIR light-driven PEC aptasensing platform against 0.01 ng mL^{-1} CEA, alpha-fetoprotein (AFP), lysozyme (Lyso; 1.0 ng mL^{-1}), human IgG (1.0 ng mL^{-1}), prostate-specific antigen (PSA; 1.0 ng mL^{-1}), thrombin (TB; 1.0 ng mL^{-1}), and mixture containing all the analytes.

The reproducibility of NIR light-driven photoelectrochemical aptasensing platform were studied toward CEA standards at different concentrations (0.1, 1.0 and 5.0 ng mL^{-1} CEA used herein) within replicates of the assay by using upconversion nanoparticles from a single batch and different synthetic batches, respectively. As indicated in Table S2 in the Supporting Information, the relative standard deviations (RSDs) were 5.6% for 0.1 ng mL^{-1}, 8.3% for 1.0 ng mL^{-1} and 6.6% for 5.0 ng mL^{-1} CEA by using the UCNs from a single batch, respectively. The synthesis-to-synthesis reproducibility of sensor materials was also investigated by using UCNs from various synthetic batches for preparation of the aptasensor. The RSDs were 8.1%, 11.4% and 10.1% toward the above-mentioned concentrations, respectively (Table S3 in the Supporting Information). The results revealed that our aptasensing strategy had good reproducibility.

In addition, we also investigated the stability of the PEC aptasensor with Ag_2S precipitate for the multiple measurements (0.01 ng mL^{-1} CEA). The RSD value was 7.4% within 10 repeated measurements (Figure S3 in the Supporting Information). Furthermore, the storage stability of $NaYF_4$:Yb,Er-based aptasensing platform were studied by storing them at 4 °C in refrigerator when not in use. The evaluation was carried out by assay 1.0 ng mL^{-1} CEA intermittently within six-week period. Experimental results indicated that the photocurrents of this aptasensor could preserve 98.1%, 96.4%, 94.6%, 94.1%, 93.7% and 93.2% of the initial signal at the 1st, 2nd, 3rd, 4th, 5th and 6th week, respectively, indicating a good stability.

Analysis of Human Serum Samples. To study the accuracy of the newly developed detection system, the as-prepared aptasensors were employed to evaluate six human serum specimens containing target CEA with different concentrations, collected from local Provincial Hospital (Fuzhou, China) according to the rules of the local ethical committee). During the measurements, all handing and processing were performed carefully, and all tools in contact with patient specimens were disinfected after use. The CEA levels were calculated according to the equation: y (nA) = 253.057 + 77.748 × log$C_{[CEA]}$ described in Figure 4B. Meanwhile, these samples were also evaluated by CEA ELISA kit. The data are shown in Table 1. The method accuracy were investigated by using a *t*-test method.[35] Therefore, there is no significant differences between two methods in the analysis of 6 clinical serum samples since all t_{exp} values were below 2.77 ($t_{crit[0.05,4]}$ = 2.77).

Table 1. Evaluation of Results for Real Samples by NIR Light-Driven Photoelectrochemical Aptasensor and ELISA Kit

	method (concentration: mean ± SD, ng mL^{-1}; n = 3)[a]		
sample no.	NIR light-driven PEC biosensor	CEA ELISA kit	t_{exp}
1	0.55 ± 0.02	0.51 ± 0.03	1.92
2	0.93 ± 0.04	0.96 ± 0.05	0.81
3	1.67 ± 0.08	1.59 ± 0.07	1.30
4	2.39 ± 0.12	2.18± 0.16	1.82
5	3.54 ± 0.18	3.73 ± 0.21	1.19
6	5.06 ± 0.24	5.26 ± 0.36	0.80

[a] The high-amount analytes were assayed with dilution.

CONCLUSIONS

In conclusion, this work reports on a NIR light-driven PEC aptasensor for sensitive determination of CEA coupling with target-triggered *in-situ* fabrication of Ag_2S nanoparticles and $NaYF_4$:Yb,Er upconversion nanotransducer. The NIR light, used as an excitation light source, possessed the extraordinary properties with strong penetration depth, near-zero photo-bleaching and low phototoxicity. $NaYF_4$:Yb,Er upconversion nanoparticles, used as the light transducer, could convert the NIR light into adjustable wavelengths by doping with different elements. The signal amplification strategy depended on the *in-situ* reaction of massive C-Ag^+-C for Ag_2S precipitate *via* target-triggered HCR. Formation of Ag_2S precipitate was allowed to absorb the well-matched light from the emissions of $NaYF_4$:Yb,Er UCNs, thus generating the photocurrent to realize the sensing protocol. Significantly, an additional merit for the *in-situ* generation of Ag_2S precipitate could absorb greatly and utilize effectively the whole Vis region from the emissions of $NaYF_4$:Yb,Er, thereby providing a "green" strategy for the development of UCNs-based NIR light-responsive PEC detection. As expected, the NIR light-driven PEC sensing platform presented high sensitivity, high selectivity and good stability. Importantly, the designed sensing platform opens an unusual platform for the future construction of NIR light-mediated PEC detection and offers a reliable mechanism for the *in-situ* fabrication of Ag_2S precipitate *via* HCR amplification.

ASSOCIATED CONTENT

Supporting Information

The Supporting Information is available free of charge on the ACS Publications website at DOI: 10.1021/acs.analchem.0000.

Material and reagent, photocurrent measurement, /SEM images and EDS (Figure S1), /control tests on Ag_2S precipitates-modified electrode (Figure S2), the stability of $NaYF_4$:Yb,Er-modified electrode with Ag_2S precipitates (Figure S3),/ comparison of analytical properties of NIR-based PEC aptasensor with other CEA detection schemes (Table S1), /reproducibility for intra-assays (Table S2), and reproducibility for inter-assay (Table S3) (PDF)

AUTHOR INFORMATION

Corresponding Author

* Phone: +86-591-2286 6125. Fax: +86-591-2286 6135. E-mail: dianping.tang@fzu.edu.cn (D. Tang).
ORCID(ID)
Dianping Tang: 0000-0002-0134-3983

Notes

The authors declare no competing financial interest.

ACKNOWLEDGMENT

We gratefully acknowledge the financial supports from the National Natural Science Foundation of China (21675029, 21874022, 21475025), and the Program for Changjiang Scholars and Innovative Research Team in University (IRT15R11)

REFERENCES

(1) Zhao, W.; Xu, J.; Chen, H. Photoelectrochemical bioanalysis: the state of the art. *Chem. Soc. Rev.* **2015**, *44*, 729-741.
(2) Zhao, W.; Xu, J.; Chen, H. Photoelectrochemical DNA biosensors. *Chem. Rev.* **2014**, *114*, 7421-7441.
(3) Qu, Y.; Duan, X. Progress, challenge and perspective of heterogeneous photocatalysts. *Chem. Soc. Rev.* **2013**, *42*, 2568-2580.
(4) Kwon,W.; Lee,G.; Do, S.; Joo, T.; Rhee, S. Size-controlled soft-template synthesis of carbon nanodots toward versatile photoactive materials. *Small* **2014**, *10*, 506-513.
(5) Josset, S.; Keller, N.; Lett, M.; Ledoux, M.; Keller, V. Numeration methods for targeting photoactive materials in the UV-A photocatalytic removal of microorganisms. *Chem. Soc. Rev.* **2008**, *37*, 744-755.
(6) Wang, S.; Zhao, L.; Bai, L.; Yan, J.; Jiang, Q.; Lian, J. Enhancing photocatalytic activity of disorder-engineered C/TiO2 and TiO2 nanoparticles. *J. Mater. Chem. A* **2014**, *2*, 7439-7445.
(7) Deng, K.; Li, L. CdS nanoscale photodetectors. *Adv. Mater.* **2014**, *26*, 2619-2635.
(8) Ali, M.; Winterer, M. ZnO nanocrystals: surprisingly 'alive'. *Chem. Mater.* **2010**, *22*, 85-91.
(9) Qin, W.; Zhang, D.; Zhao, D.; Wang, L.; Zheng, K. Near-infrared photocatalysis based on YF_3:Yb^{3+},Tm^{3+}/TiO_2 core/shell nanoparticles. *Chem. Commun.* **2010**, *46*, 2304-2306.
(10) Wang, K.; Zhang, R.; Sun, N.; Li, X.; Wang, J.; Cao, Y.; Pei, R. Near-infrared light-driven photoelectrochemical aptasensor based on the upconversion nanoparticles and TiO2/CdTe heterostructure for detection of cancer cells. *ACS Appl. Mater. Interfaces* **2016**, *8*, 25834-25839.
(11) Tang, Y.; Di, W.; Zhai, X.; Yang, R.; Qin, W. NIR-responsive photocatalytic activity and mechanism of $NaYF_4$:Yb,Tm@TiO_2 core-shell nanoparticles. *ACS Catal.* **2013**, *3*, 405-412.
(12) Wang, J.; Tanner, P. Upconversion for white Light generation by a single compound. *J. Am. Chem. Soc.* **2010**, *132*, 947-949.
(13) Han, S.; Deng, R.; Xie, X.; Liu, X. Enhancing luminescence in lanthanide-doped upconversion nanoparticles. *Angew. Chem., Int. Ed.* **2014**, *53*, 11702-11715.
(14) Greybush, N.; Saboktakin, M.; Ye, X.; Della Giovampaola, C.; Oh, S.; Berry, N.; Engheta, N.; Murray, C.; Kagan, C. Plasmon-enhanced upconversion luminescence in single nanophosphor-nanorod heterodimers formed through template-assisted self-assembly. *ACS Nano* **2014**, *8*, 9482-9491.
(15) Hilderbrand, S.; Weissleder, R. Near-infrared fluorescence: application to in vivomolecular imaging. *Curr. Opin. Chem. Biol.* **2010**, *14*, 71-79.
(16) Liu, Q.; Yang, T.; Feng, W.; Li, F. Blue-emissive upconversion nanoparticles for low-power-excited bioimaging in vivo. *J. Am. Chem. Soc.* **2012**, *134*, 5390-5397.
(17) Bai, L.; Jiang, W.; Gao, C.; Zhong, S.; Zhao, L.; Li, Z.; Bai, S. Facet engineered interface design of $NaYF_4$:Yb,Tm upconversion nanocrystals on BiOCl nanoplates for enhanced near-infrared photocatalysis. *Nanoscale* **2016**, *8*, 19014-19024.
(18) He, M.; Liu, Z. Paper-based microfluidic device with upconversion fluorescence assay. *Anal. Chem.* **2013**, *85*, 11691-11694.
(19) Idris, N.; Jayakumar, M.; Bansal, A.; Zhang, Y. Upconversion nanoparticles as versatile light nanotransducers for photoactivation applications. *Chem. Soc. Rev.* **2015**, *44*, 1449-1478.
(20) Li, Y.; Liu, X.; Yang, X.; Lei, H.; Zhang, Y.; Li, B. Enhancing upconversion fluorescence with a natural bio-microlens. *ACS Nano* **2017**, *11*, 10672-10680.
(21) Xu, Z.; Quintanilla, M.; Vetrone, F.; Govorov, A.; Chaker, M.; Ma, D. Harvesting lost photons: plasmon and Uuconversion enhanced broadband photocatalytic activity in core@shell microspheres based on lanthanide-doped $NaYF_4$, TiO_2, and Au. *Adv. Funct. Mater.* **2015**, *25*, 2950-2960.
(22) Qiu, Z.; Shu, J.; Tang, D. Near-infrared-to-ultraviolet light-mediated photoelectrochemical aptasensing platform for cancer biomarker based on core-shell $NaYF_4$:Yb,Tm@TiO_2 upconversion microrods. *Anal. Chem.* **2018**, *90*, 1021-1028.
(23) Du, Y.; Xu, B.; Fu, T.; Cai, M.; Li, F.; Zhang, Y.; Wang, Q. Near-infrared photoluminescent Ag_2S quantum dots from a single source precursor. *J. Am. Chem. Soc.* **2010**, *132*, 1470-1471.
(24) Shen, H.; Jiao, X.; Oron, D.; Li, J.; Lin, H. Efficient electron injection in non-toxic silver sulfide (Ag_2S) sensitized solar cells. *J. Power Sources* **2013**, *240*, 8-13.
(25) Zhang, Y.; Hong, G.; Zhang, Y.; Chen, G.; Li, F.; Dai, H.; Wang, Q. Ag_2S quantum dot: a bright and biocompatible fluorescent nanoprobe in the second near-infrared window. *ACS Nano* **2012**, *6*, 3695-3702.
(26) Zimmer, R.; Thomas, P. Mutations in the carcinoembryonic antigen gene in colorectal cancer patients: implications on liver metastasis. *Cancer Res.* **2001**, *61*, 2822-2826.
(27) Hine, K.; Booth, S.; Leonard, J.; Dykes, P. Carcinoembryonic antigen concentrations in undiagnosed patients. *Lancet* **1978**, *2*, 1337-1340.
(28) Lai, G.; Wu, J.; Ju, H.; Yan, F. Streptavidin-functionalized silver-nanoparticle-enriched carbon nanotube tag for ultrasensitive multiplexed detection of tumor markers. *Adv. Funct. Mater.* **2011**, *21*, 2938-2943.
(29) Wu, Y.; Zhang, X.; Zhang, D.; Zhang, C.; Li, J.; Wu, Y.; Song,

Z.; Yu, R.; Tan, W. Quench-shield ratiometric upconversion luminescence nanoplatform for biosensing. *Anal. Chem.* **2016**, *88*, 1639-1646.

(30) Chen, H.; Li, H.; Lin, J. Determination of ammonia in water based on chemiluminescence resonance energy transfer between peroxymonocarbonate and branched $NaYF_4$:Yb^{3+}/Er^{3+} nanoparticles. *Anal. Chem.* **2012**, *84*, 8871-8879.

(31) Huang, S.; Gu, L.; Miao, C.; Lou, Z.; Zhu, N.; Yuan, H.; Shan, A. Near-infrared photocatalyst of Er^{3+}/Yb^{3+} codoped (CaF_2@TiO_2) nanoparticles with active-core/active-shell structure. *J. Mater. Chem. A* **2013**, *1*, 7874-7879.

(32) Jarosz, A.; Yep, T.; Mutus, B. Microplate-based colorimetric detection of free hydrogen sulfide. *Anal. Chem.* **2013**, *85*, 3638-3643.

(33) Gulzar, A.; Xu, J.; Yang, P.; He, F.; Xu, L. Upconversion processes: versatile biological applications and biosafety. *Nanoscale* **2017**, *9*, 12248-12282.

(34) Wu, J.; Fu, Z.; Yan, F.; Ju, H. Biomedical and clinical applications of immunoassays and immunosensors for tumor markers. *TRAC-Anal. Chem.* **2007**, *26*, 679-688.

(35) Qiu, Z.; Shu, J.; Tang, D. Bioresponsive release System for visual fluorescencedetection of carcinoembryonic antigen from mesoporous silica nanocontainers mediated optical color on quantum dot-enzyme-impregnated paper. *Anal. Chem.* **2017**, *89*, 5152-5160.

For only TOC

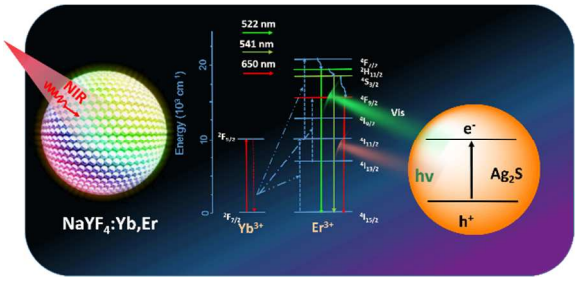
522 nm
541 nm
650 nm
NIR
Energy (10^4 cm^{-1})
20
10
0
Vis
e$^-$
hv
Ag_2S
h$^+$
$NaYF_4$:Yb,Er
Yb^{3+}
Er^{3+}